Synthesis, Characterization and Cold Workability of Cast Copper-Magnesium-Tin Alloys

AGUSTÍN EDUARDO BRAVO BÉNARD, DAVID MARTÍNEZ HERNÁNDEZ, JOSÉ GONZALO GONZÁLEZ REYES, ARMANDO ORTIZ PRADO, and RAFAEL SCHOUWENAARS FRANSSENS

The use of Mg as an alloying element in copper alloys has largely been overlooked in scientific literature and technological applications. Its supposed tribological compatibility with iron makes it an interesting option to replace Pb in tribological alloys. This work describes the casting process of high-quality thin slabs of Cu-Mg-Sn alloys with different compositions by means of conventional methods. The resulting phases were analyzed using X-ray diffraction, scanning electron microscopy, optical microscopy, and energy dispersive X-ray spectroscopy techniques. Typical dendritic α-Cu, eutectic $Cu_2Mg(Sn)$ and eutectoid non-equilibrium microstructures were found. Tensile tests and Vickers microhardness show the excellent hardening capability of Mg as compared to other copper alloys in the as-cast condition. For some of the slabs and compositions, cold rolling reductions of over 95 pct have been easily achieved. Other compositions and slabs have failed during the deformation process. Failure analysis after cold rolling reveals that one cause for brittleness is the presence of casting defects such as microshrinkage and inclusions, which can be eliminated. However, for high Mg contents, a high volume fraction of the intermetallic phase provides a contiguous path for crack propagation through the connected interdendritic regions.

DOI: 10.1007/s11661-013-1993-3

I. INTRODUCTION

Cu-Pb alloys with low Sn content have been used for the last 100 years as the functional material in journal bearings. The mechanical resistance comes from the Cu-Sn matrix, while the Pb phase provides the higher tribological compatibility with iron. Considering that these alloys have served their purpose quite well during this time, research, and development of high strength triboalloys has received very little attention. However, the actual trends to reduce energy costs by raising machine efficiency and lowering friction and wear, as well as the concern about the toxicity of Pb, create demand for higher strength and environment-friendly triboalloys.[1]

Based on Rabinowicz's[2] tribological compatibility studies and considering that either steel or cast iron are used for the crankshaft and other components that may come in contact with the journal bearing's functional alloy, the possible elements that could replace Pb are In, Cd, Ag, Zr, Bi, Sn, and Mg. The first two are toxic, Ag and Zr are relatively expensive and Bi does not look to be a very promising solution.[3] Cu-Mg alloys are already used in similar applications,[4–8] which means that Mg may be another alternative to substitute Pb in leaded tin bronzes for improved tribological properties and environmental safety.

The preferred method to manufacture Al-Sn alloys used for journal bearings is thin slab casting followed by cold rolling.[9,10] This process is relatively simple and cost-effective. Powder metallurgy is used to manufacture Cu-Pb journal bearings. However, the latter is more difficult to accomplish in Mg containing alloys due to this elements high oxygen affinity at high temperatures. This affinity also affects the casting process. For Mg castings, there has been an enormous amount of research to find an efficient melt protection alternative to SF_6 which is highly contaminating.[11]

The amount of Mg used in commercial Cu-Mg alloys is usually less than 1 pct in weight.[4–8] This results in a very small volume fraction of the second phase due to the solubility of Mg in Cu. In Cu-Sn alloys, the formability is limited for Sn contents above 10 pct.[12] Even though the Cu-Sn binary phase diagram has been well studied and the thermodynamic assessment recently done by Liu *et al.*[13] appears to be the most reliable,[14,15] slight differences still appear in the literature. The most recent experimental study was done by Fürtauer *et al.*[16] in which they report the latest version of the Cu-Sn binary phase diagram. This study was backed up by Li *et al.*[17] with a thermodynamic assessment. However, it is well established that the

AGUSTÍN EDUARDO BRAVO BÉNARD, DAVID MARTÍNEZ HERNÁNDEZ, ARMANDO ORTIZ PRADO, and RAFAEL SCHOUWENAARS FRANSSENS, Professors, are with the Departamento de Materiales y Manufactura, Facultad de Ingeniería, Edificio O, Universidad Nacional Autónoma de México, Avenida Universidad 3000, 04510 Mexico DF, Mexico. Contact e-mail: agsterix@yahoo.com JOSÉ GONZALO GONZÁLEZ REYES, Professor, is with the Instituto de Investigaciones en Materiales, Universidad Nacional Autónoma de México, Circuito Exterior, Ciudad Universitaria, Coyoacán, 04510 Mexico DF, Mexico.

Manuscript submitted August 28, 2012.
Article published online September 17, 2013

solubility of Sn in Cu is highly temperature-dependent and that Cu-Sn alloys rarely follow an equilibrium solidification route.[15,18,19] Furthermore, very little information about the ternary Cu-Mg-Sn phase diagram is available. A review of this ternary system was given by Rokhlin and Lysova,[20] confirming the stability of a ternary Cu_4MgSn phase. This study does not present thermodynamic data which allow to calculate its enthalpy of formation or any other data required to introduce this phase in the thermodynamic assessment of the phase diagram. The experimental data which they considered were relatively old; the most recent ones published by Vicente *et al.*[21,22] from the 1990s, while the oldest date as far back as the 1920s. A thermodynamic optimization of the ternary system was recently done by Miettinen and Vassilev.[23] They found a reasonable correlation between the calculated and previously reported experimental data using the assessed binary sub-systems and considering the Cu_4MgSn phase as stoichiometric. The experimental results presented in this work will contribute further to the understanding of the metallurgical aspects of the Cu-Mg-Sn system in the Cu-rich corner and, more specifically, on the appearance of the Cu_4MgSn phase. As the solidification processes reported here are non-equilibrium, care should be taken when interpreting the data in relationship with proposed phase diagrams.

After considering the available options, casting followed by cold rolling was chosen to produce and characterize the proposed Cu-Mg-Sn alloys. Mg is used as an alloying element and must be put into the liquid bronze bath just before pouring. A good melt protection is necessary as the solid Mg tends to float up to the surface and completely oxidize. A detailed description of the casting technique to obtain thin slabs with very low porosity and the desired compositions is presented. This process was designed to use only the most simple and conventional tools and still provide a good protection against Mg loss due to oxidation. An analysis of the resulting microstructures using optical and scanning electron microscopy, X-ray diffraction (XRD), and energy dispersive X-ray spectrometry is shown. The fracture zones of thin slabs that failed during cold-rolling and of tensile specimens of the as-cast material are analyzed as well.

II. EXPERIMENTAL PROCEDURE

As a starting point, the four basic compositions shown in Table I were chosen. To produce the alloys, a graphite crucible was used in a gas furnace. Thin slabs were cast in a permanent horizontal steel mold. Electrolytic Cu and industrial purity Sn with Pb impurities were used as the starting materials. Electrolytic Mg was covered with graphite powder. The molten bronze metal was also covered with a thin layer of graphite powder and the Mg was plunged to the bottom of the melt using a graphite tube and a steel plunger. This minimizes Mg loss due to the oxidation by direct contact with air. The melt was degassed using commercial $CaCO_3$ tablets for 1 to 2 minutes. All tools were preheated to ~773 K (500 °C). Cooling curves were obtained using type-K thermocouples and cross-checked with an optical pyrometer as described in a previous paper.[19]

The resulting phases after casting were determined using a Siemens D5000 diffractometer using cobalt-Kα-radiation and an Oxford energy dispersive X-ray spectroscopy (EDS) spectrometer. Metallographic samples for scanning electron microscopy (SEM) and optical microscopy (OM) were prepared using standard techniques. Etching of specimens for OM was done using Keller's reagent, immersing for ~30 seconds. Tensile specimens of the as-cast thin slabs were machined in a numerically controlled vertical mill according to ASTM-E8. Sub-size specimens were used, resulting in gage lengths of 25 mm, widths of 6 mm, and variable thickness of ~2 mm. Tensile tests were performed in a Shimadzu universal test machine, using an initial strain rate of 3.33×10^{-3} s^{-1}. Vickers hardness was measured using an Instrumented Nanovea Microhardness Tester using a load of 10 N and a dwell time of 10 seconds and between 25 to 40 indentations per sample. The deformation process was carried out at room temperature using reductions of 2, 4, 6, and 8 pct in the first four passes and a series of subsequent reductions of 10 pct per step. The initial thickness of the slabs was ~2 cm with variable length and width. A rolling speed of 7.62 m/min and 127 mm diameter rolls were used. This cold rolling procedure minimizes material loss due to rolling defects in other commercially used triboalloys.[9]

Table I. Nominal Compositions, Measured Compositions and Number of Slabs

	Composition (Wt Pct)				Measured Composition* (Wt Pct)					
Alloy Designation	Cu	Mg	Sn	Slab	Mg	Sn	Pb	Fe	Al	V
Cu-1Mg-1Sn	98	1	1	1	1.07	1.09	0.26	0.02	—	—
				2	1.05	1.12	0.25	0.01	—	—
Cu-1Mg-5Sn	94	1	5	1	1.09	4.16	0.20	—	0.06	0.18
				2	0.98	4.90	0.21	—	0.04	—
Cu-5Mg-1Sn	94	5	1	1	5.37	0.30	0.24	0.10	—	—
				2	5.54	0.81	0.23	0.03	—	—
Cu-5Mg-5Sn	90	5	5	1	5.17	4.34	0.21	—	—	—
				2	5.33	3.71	0.20	—	—	—
				3	5.33	4.82	0.21	—	—	—
				4	5.88	4.26	0.22	0.04	—	—

*Cu balance.

Fracture surfaces and cross-sections of both tensile specimens and low ductility cold rolled samples were analyzed using a Philips XL-20 SEM with a tungsten filament and an Oxford EDS spectrometer.

III. RESULTS AND DISCUSSION

Thin slabs of the desired composition were cast under controlled conditions. Table I indicates the nominal alloy composition, the number of cast slabs, and the measured chemical composition. Table II shows the measured Vickers hardness, the tensile specimens and the average measured parameters from tensile tests.

A. *Casting Process*

The presence of Mg makes the melt highly sensitive to oxidation and consequently high porosity is common. A series of preliminary tests were useful to avoid the most severe casting defects. Correct degassing of the melt and a well-controlled pouring speed are essential to obtain acceptable results. With an adequate control of the process, Mg oxidation and micropores can be minimized. Macroscopic observation of the cross-section of thin slabs reveals a higher porosity towards the top. Microshrinkage caused by the lack of liquid phase during solidification appeared in some samples. The low melting point [505 K (232 °C)] of Sn results in higher microsegregation for the 5 pct Sn compositions.

B. *Microstructural Analysis*

Microscopic observation shows a dendrite-type microstructure, typical of cast bronze and copper alloys, with interdendritic phases of different types and compositions. Elemental chemical analyses confirm that the compositions are close to the expected ones. Figure 1 shows the resulting microstructures for the four compositions studied. Local EDS analyses show a dendrite composition of Cu with Mg and Sn at the solid solubility limit. Segregation was confirmed by atomic number contrast using backscattered electrons, especially for the 5 pct Sn compositions. Graphite inclusions were found in some of the samples as well.

1. *Cu-1Mg-1Sn*

For the Cu-1Mg-1Sn composition, a single phase should be obtained under equilibrium conditions. A small fraction of second phase was found in the interdendritic regions as a eutectic mixture of Cu and Cu_2Mg (Figure 1(a)). The second phase found in binary copper-tin alloys under non-equilibrium solidification is usually the BCC β phase.[24] The δ phase is sometimes found for higher Sn content.[14,18] Neither of these phases was seen in any of the samples.

2. *Cu-1Mg-5Sn*

For the Cu-1Mg-5Sn samples, the non-equilibrium solidification results in the coring of dendrites (Figure 1(b)) and a fine eutectoid microstructure, which can be seen in more detail in Figure 2(a). There is evidence of strong segregation and a peritectic reaction followed by a eutectoid reaction during solidification. This micrograph is interpreted as presenting a reaction border which would be characteristic of the presence of a peritectic reaction. In this case, the very fine, regular, rod-like microstructure must be interpreted as a eutectoid decomposition of a three-component analogue of the β or γ phase found in the binary Cu-Sn diagram.[16,17]

The calculated composition of the interdendritic regions is very close to 6:2:1 (Cu:Mg:Sn). A precise local composition analysis could not be made because of the extremely fine microstructure (particle sizes $<0.5\ \mu m$). However, considering that these regions consist of Cu_2Mg and an intermetallic phase in a 1:1 ratio, an estimation of the composition of the intermetallic compound is close to that of Cu_4MgSn.

Micropores appear to be randomly distributed in the interdendritic zones. Figure 2(b) shows a microshrinkage pattern associated with this phenomenon between two dendrite arms.

3. *Cu-5Mg-1Sn*

A homogeneous mixture of (Cu) + Cu_2Mg was found in the interdendritic regions of the Cu-5Mg-1Sn compositions. An optical micrograph is shown in Figure 1(c) (inset), revealing the dendritic microstructure. The Cu-5Mg-1Sn alloy showed the lowest segregation of all the compositions studied in this work. A large volume fraction of the Cu_2Mg intermetallic compound results in a connected interdendritic zone. During cold work, crack propagation follows this brittle phase and results in crack growth, eventually leading to failure. By limiting the connected zones between dendrites, crack propagation is supposed to be stopped at the ductile dendrites.

4. *Cu-5Mg-5Sn*

The Cu-5Mg-5Sn alloy shows a eutectic microstructure with some regions enriched in Sn due to higher microsegregation (brighter zones in Figure 1(d)) embedded in a Cu_2Mg matrix (darker zones). EDS line scans reveal a Cu_2Mg composition along the interdendritic

Table II. Measured Mechanical Properties, Average Vickers Hardness (HV), Tensile Specimens (TS) and Average Measured Parameters (with Standard Deviation) From Tensile Tests

Alloy	HV (MPa)	TS	$\sigma_{0.2}$ (MPa)	σ_{max} (MPa)	ε_{hom} (pct)	ε_{max} (pct)
Cu-1Mg-1Sn	689 ± 72	8	69.7 ± 11	194.3 ± 38	14.08 ± 7	14.44 ± 7
Cu-1Mg-5Sn	911 ± 162	3	112.4 ± 13	208.3 ± 4	4.06 ± 0.3	4.18 ± 0.4
Cu-5Mg-1Sn	2239 ± 207	0	—	—	—	—
Cu-5Mg-5Sn	2277 ± 308	0	—	—	—	—

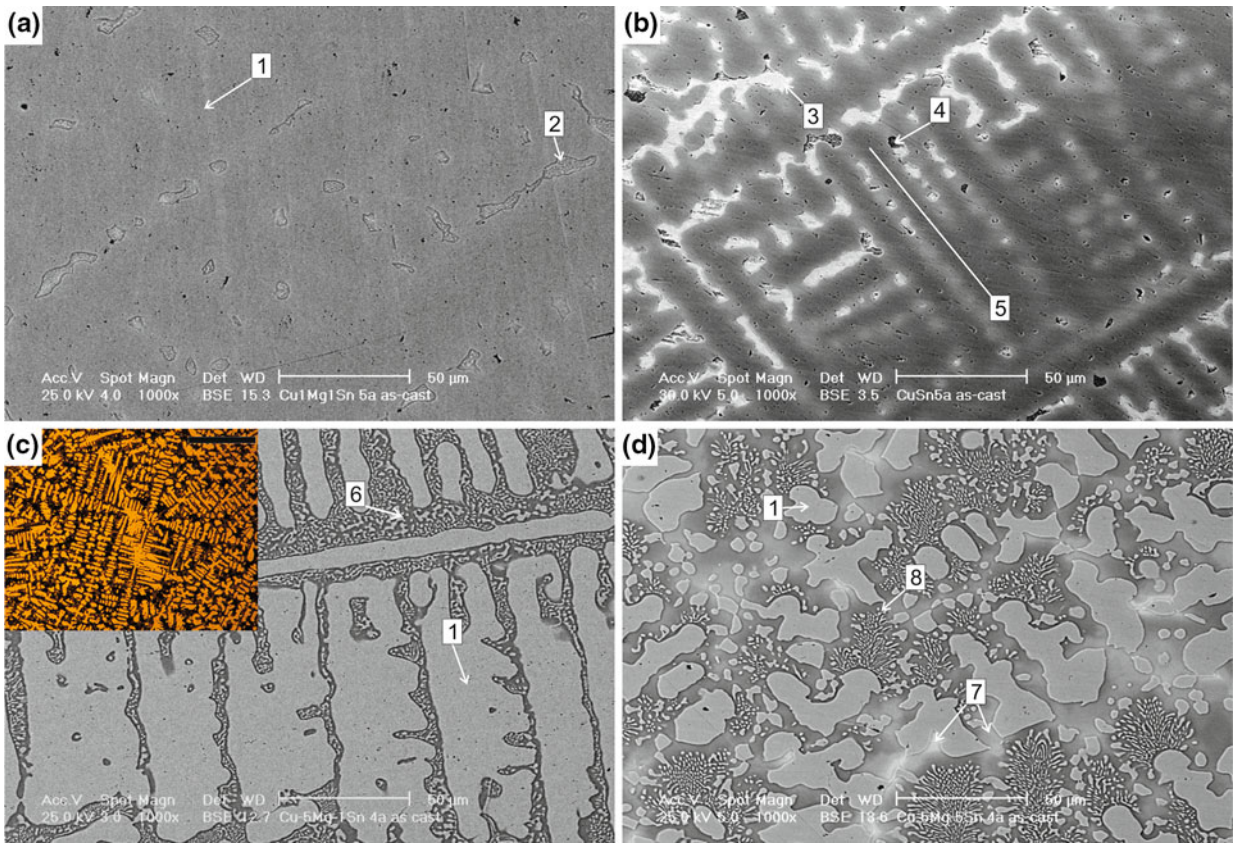

Fig. 1—As-cast microstructures for: (*a*) Cu-1Mg-1Sn, (*b*) Cu-1Mg-5Sn, (*c*) Cu-5Mg-1Sn (inset: OM image, scale bar is 400 μm), (*d*) Cu-5Mg-5Sn. 1. (Cu) dendrite arms, 2. Eutectic mixture of (Cu) + Cu_2Mg, 3. Fine (unresolved) eutectoid mixture of (Cu) + Cu_4MgSn, 4. Microshrinkage, 5. Cored (Cu) dendrite, 6. Homogeneous eutectic mixture of (Cu) + Cu_2Mg, 7. $Cu_2Mg(Sn)$ with high Sn content, 8. Eutectic mixture of (Cu) + $Cu_2Mg(Sn)$.

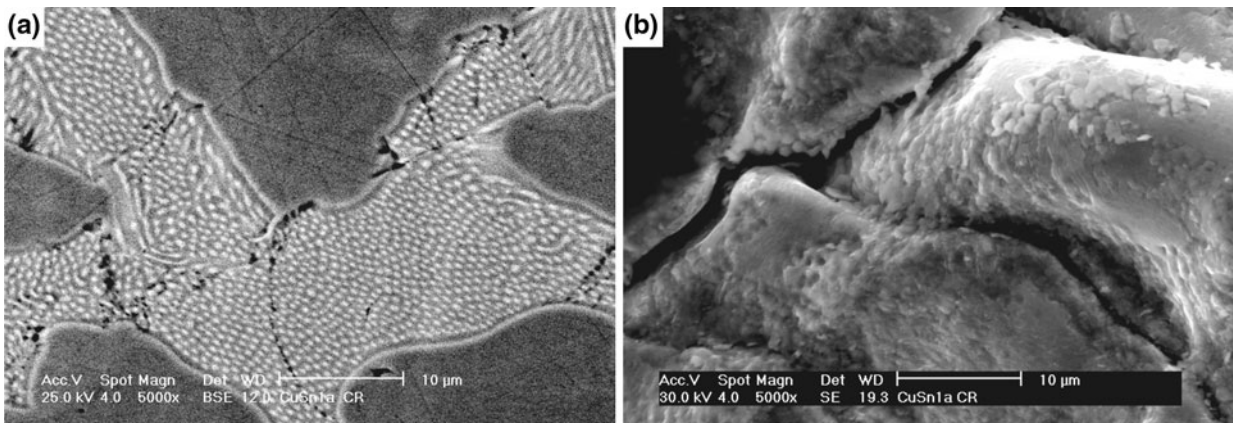

Fig. 2—SEM image showing different views of a Cu-1Mg-5Sn sample after a cold-rolling reduction of 4 pct. (*a*) A fine and regular interdendritic microstructure with a reaction border along the dendrites suggests a peritectic reaction previous to the eutectoid reaction. Microcracks are already propagating through the brittle phases. (*b*) Interdendritic region showing typical patterns associated with the lack of liquid and microshrinkage during solidification. The lack of cohesion between the dendrites favors crack propagation during cold-rolling.

regions with varying Sn content. This is consistent with the ternary phase diagram which shows some solubility of Sn for this intermetallic compound.[20] Considering that the solidification range becomes larger with increasing Sn content (~100 K for 5 pct Sn compared to 30 K for 1 pct Sn in the binary phase diagram), segregation becomes more significant. The appearance of phases with different compositions compared to the ones expected in

equilibrium is inevitable for the cooling speed achieved using this casting process (~300 K/min). However, no reaction (eutectoid or ordering transition[13,16,17]) near the 859 K (586 °C) temperature was seen during the analysis of the cooling curves[19] and again, no β or δ phases were found.

C. *X-Ray Diffraction Analysis*

The results of the XRD experiments show the characteristic spectrum for the three compositions with higher Mg/Sn ratio in which two phases are formed, α-Cu and Cu_2Mg (Figure 3(a)). For the Cu-1Mg-5Sn composition (Mg/Sn ratio = 0.2), a third phase is present. This is most likely the Cu_4MgSn phase which is very similar to the Cu_2Mg phase.[25,26] The diffraction patterns of these two phases almost completely overlap in the whole experimental spectrum, except for the (200) reflection, making the identification of Cu_4MgSn somewhat difficult. This (200) peak was only present for the Cu-1Mg-5Sn composition (Figure 3(b)). Furthermore, the Cu_4MgSn presence is also evidenced by the (220) peak, which shows a shoulder, indicating the reflections of the Cu_4MgSn and Cu_2Mg peaks at 36.04 and 36.07 deg (2θ), respectively. This suggests that the third phase found in the metallographic analysis of the Cu-1Mg-5Sn composition is indeed Cu_4MgSn, confirming the assumption of a $Cu_2Mg + Cu_4MgSn$ eutectoid mixture. This is shown by the characteristic reflection of Cu_4MgSn (200) alongside the Cu_2Mg phase in Figure 3(b). The absence of a (200) reflection and a shoulder in the (220) peak in Figure 3(a) further suggests that the phase formed in the Cu-5Mg-5Sn compositions is $Cu_2Mg(Sn)$.

The binary phase shows significant solid solubility for Sn.[20] There are four available octahedral spaces in which a Mg atom can be substituted by a Sn atom and, therefore, the $Cu_2Mg(Sn)$ can come close in composition and lattice parameters to Cu_4MgSn but lacks this (200) diffraction peak. These two phases belong to different space groups, but they are both Laves phases and so are very hard and brittle. By controlling their volume fraction and morphology, their hardening effect can be very efficient.

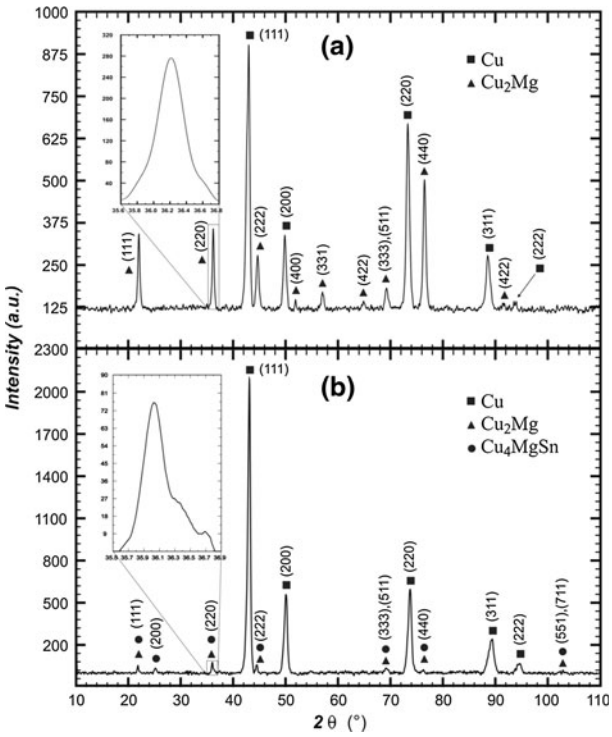

Fig. 3—XRD patterns for: (*a*) Cu-5Mg-5Sn alloy showing that only two phases (Cu and Cu_2Mg) are formed. Inset: The (220) reflection shows a symmetric peak. (*b*) Cu-1Mg-5Sn alloy showing the (200) Cu_4MgSn reflection. Inset: The (220) reflection shows a typical asymmetry with a shoulder, indicating the overlapping of the Cu_4MgSn and Cu_2Mg peaks at 36.04 and 36.07 deg (2θ) respectively.

D. *Mechanical Properties*

The mechanical properties show a broad variation which is common for as-cast materials. The average Vickers hardness values and standard deviation are shown in Table II. These values are in the range of most high-copper alloys and leaded-tin bronzes.[12] There is, however, a very significant hardness contribution with higher Mg content. The Vickers hardness for the 5 pct Mg compositions is very high, in the range of heat-treated high-copper alloys.[12] The use of these materials for journal bearings requires a rolling process, which is impossible due to the presence of the contiguous brittle phase. However, for other tribological applications, these materials could also be used in the as-cast condition, taking advantage of their high strength. It shall be noted that, even if the materials are described as brittle, this is with reference to metallic materials. The typical diagonal cracks observed in truly brittle ceramics[27,28] are not present in the Vickers indents of the most brittle material studied here (Cu-5Mg-5Sn), although some cracking of the intermetallic phase does occur (Figure 4).

Tensile test results are presented in Figure 5. For the 5 pct Mg alloys, no reliable tensile specimens could be manufactured due to the fragility of the material. For the Cu-1Mg-1Sn composition, tensile curves from two different slabs are shown. The variability of the curves is typical for as-cast materials. In some of the samples,

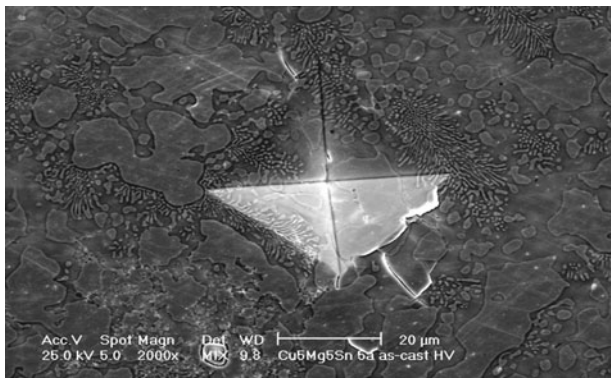

Fig. 4—Vickers indent for the Cu-5Mg-5Sn composition showing small cracks in the interdendritic region.

there is an evident premature fracture caused by the small casting defects. However, the curves show a reasonable repeatability within experimental error. A consistent work hardening is seen for all curves, resulting in maximum tensile stresses of over 150 MPa and average ductility of over 14 pct. For the Cu-1Mg-5Sn, the results shown are only for one of the slabs. Here, tensile samples tended to break in the clamps of the testing machine, due to the reduced ductility of the material and, in one of the slabs, a higher amount of casting defects. However, the three curves shown in Figure 5 for this composition indicate that the contribution to the yield strength from Sn is significant and the 4 pct average ductility is enough to start the cold rolling process.

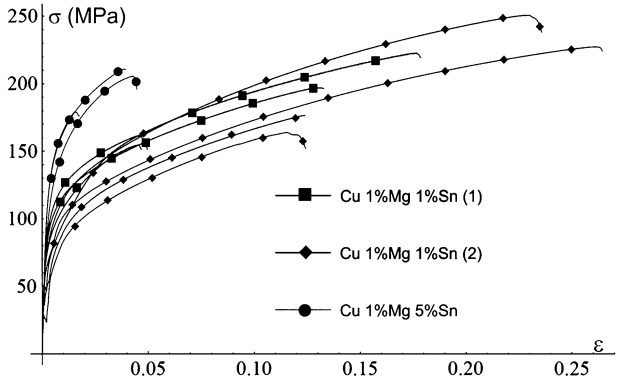

Fig. 5—Tensile curves for the Cu-1Mg-1Sn and Cu-1Mg-5Sn compositions. (1) and (2) indicate samples obtained from different slabs of the same composition.

The fracture surfaces of tensile specimens show a combined ductile and brittle fracture. The former can be seen in Figure 6, where the fracture zone of a Cu-1Mg-1Sn specimen is shown. The grain distribution is revealed through the primary dendrite arms (Figure 6(a)). A closer look shows a dimple pattern typical of ductile fracture (Figure 6(b)). In other specimens, the shrinkage cavities resulted in a higher fraction of brittle fracture. The fracture surfaces for Cu-1Mg-5Sn alloys show necking and ductile fracture (Figure 7(a)). In some samples, however, the lack of cohesion between dendrites is evident, resulting in a higher fraction of brittle fracture (Figure 7(b)).

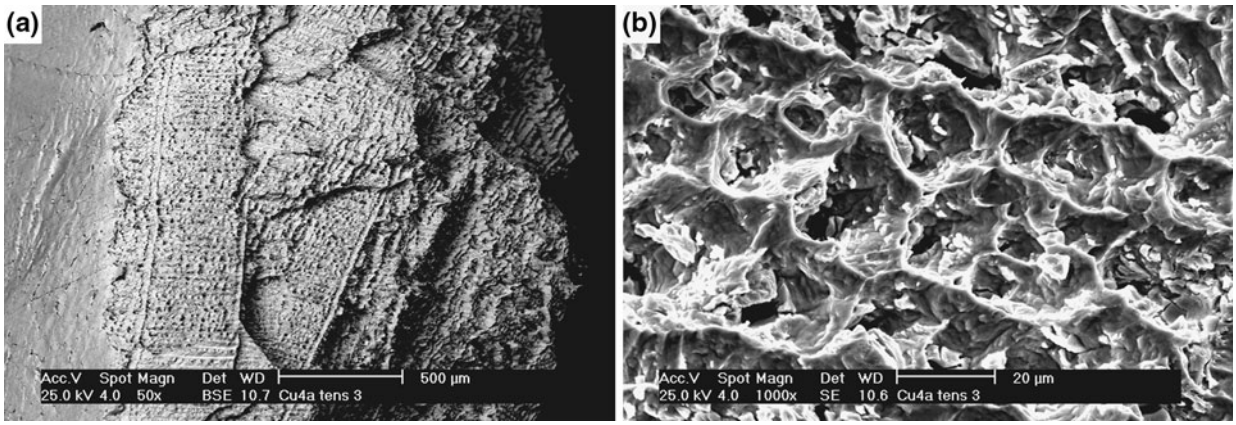

Fig. 6—Fracture surface of a Cu-1Mg-1Sn tensile specimen showing: (*a*) different grains, characterized by the primary dendrite arm, (*b*) detail showing a dimple pattern typical of ductile fracture.

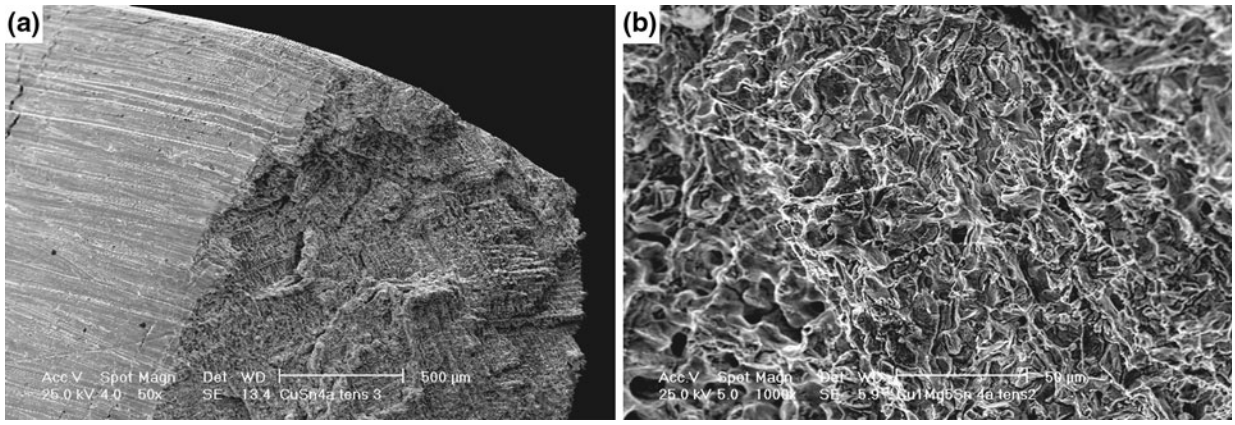

Fig. 7—Fracture surface of a tensile sample for a Cu-1Mg-5Sn alloy showing: (*a*) necking zone, (*b*) detail showing a higher fraction of brittle fracture.

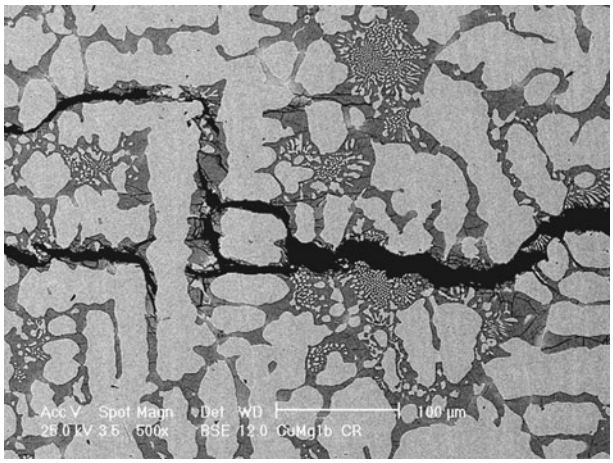

Fig. 8—Crack propagation along the interdendritic region of a Cu-5Mg-1Sn alloy after a 6 pct reduction. The connected Cu_2Mg phase allows the cracks to propagate, resulting in material failure.

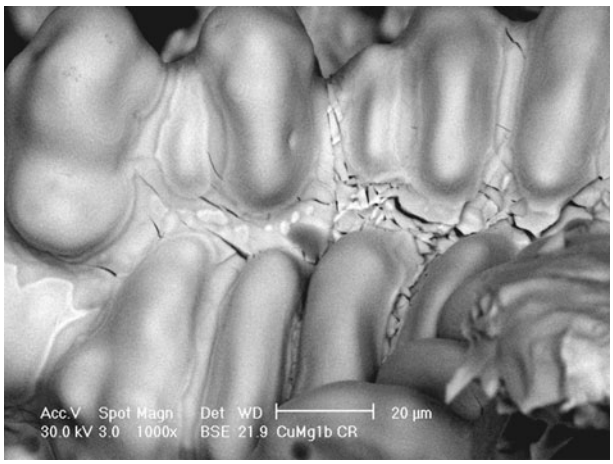

Fig. 9—Fracture surface of the sample shown in Fig. 8. Interdendritic regions are completely fractured while the (ductile) dendrites appear undamaged.

E. *Cold Rolling Process and Failure Analysis*

Cold rolling of the thin slabs was only possible for alloys with low Mg content. Reductions of 95 pct or more were achieved without any annealing process while the material remains ductile. For the 5 pct Mg alloys, after the 6 pct reduction step, the thin slabs had completely fractured. SEM observation of the fracture surfaces reveals that the cracks propagate through the intermetallic phase, shown in Figures 8 and 9. The ductile dendrites appear intact, while the interdendritic regions which contain the intermetallic phase are completely fractured.

For the Cu-1Mg-5Sn alloy, some ingots were still ductile after a 95 pct reduction, but others fractured after only a few rolling steps. Closer inspection of the fractured samples and the corresponding ingots show that the interdendritic zones fracture during cold-rolling (Figure 10). Samples that could be rolled presented a lower amount of this interdendritic structure than the ones that failed, which presented a contiguous brittle structure that allows cracks to propagate. A second factor is that ingots with a high content of interdendritic structure also show higher porosity and extended fissures due to microshrinkage along the dendrite arms. The variation in amount of interdendritic material is directly related to the amount of segregation and therefore to the cooling velocity of the ingots. The effect of cooling speed on segregation and microporosity is currently being studied.

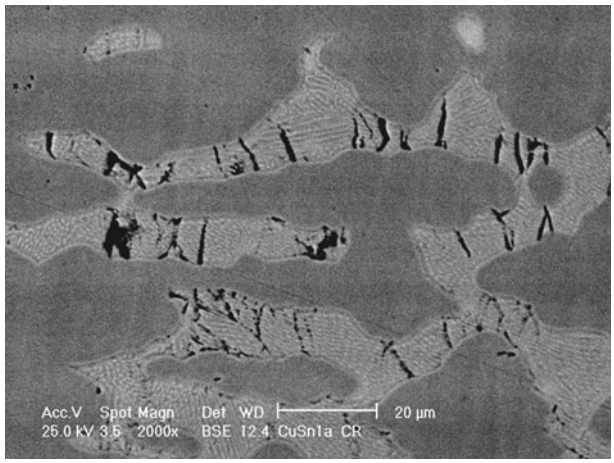

Fig. 10—After a 6 pct reduction the interdendritic regions of one of the Cu-1Mg-5Sn ingots show fractures perpendicular to the rolling direction.

This shows that the casting process and the quality of the slabs is a crucial factor for the success of the rolling process, especially for the Cu-1Mg-5Sn alloy, which appears to present a limiting condition when cold-workability is concerned. Technological defects during the casting process are then the principal causes of failure during cold-rolling for this particular composition. Isolated interdendritic regions result in ductile alloys. An optimal compromise between the hardening effect of the second phase and its volume fraction and morphology will result in a resistant, ductile alloy. The addition of other alloying elements can also be investigated in the future.

IV. CONCLUSIONS

Thin slab casting of Cu-Mg-Sn alloys has been successfully achieved using conventional equipment at a low cost. The microstructures consist mainly of two phases: α-Cu dendrites and a eutectic interdendritic region with Cu_2Mg and, for the Cu-1Mg-5Sn a eutectoid interdendritic mixture of Cu_2Mg and Cu_4MgSn Laves phases. Mechanical properties show promising results and an optimized ratio of ductile (Cu) to hard Cu_2Mg and Cu_4MgSn with isolated interdendritic zones could result in high strength, high ductility alloys. Low Mg contents result in a ductile material and cold-rolling reductions of over 95 pct. Technological defects such as inclusions, porosity and microshrinkage are the primary reason for failure during cold rolling and must be

avoided. Cracks initiate along these defects and propagate along the brittle intermetallic phases. For the 5 pct Mg alloys, the morphology of the second phase impedes plastic deformation of the alloy. Tensile fracture surfaces of the 1 pct Mg compositions show both ductile and brittle failure.

It can be concluded that the technological aspects of the casting and cold-rolling processes of these new alloys have been mastered. To determine the limits, in terms of composition, which allow cold-rolling of the slabs, a more complete study of the physical metallurgy of these alloys is being made. The effect of cooling speed on segregation and casting defects is currently being studied.

ACKNOWLEDGMENTS

The authors would like to thank the technical support of G. Alvarez, E. Ramos, I. Cueva, R. Cisneros, and J. Romero. Financial support was granted by CONACyT in project number CONACYT-SEP 168041 and Ph.D. Scholarship 175681. The work was also supported by DGAPA projects PAPIIT IN116612 and PE103312.

REFERENCES

1. A.E. Bravo, H.A. Durán, V.H. Jacobo, A. Ortiz, and R. Schouwenaars: *Wear*, 2013, vol. 302 (1–2), pp. 1528–35.
2. E. Rabinowicz: *ASLE Trans*., 1971, vol. 14 (3), pp. 198–205.
3. K. Sakai, K. Zushi, M. Sugita, and H. Ishikawa: *SAE Technical Paper*, 2004-01-1600, 2004.
4. K. Hiromitsu, K. Kazuma, A. Seigi, and H. Hiroyoshi: U.S. Patent, US 2006 0157167 A1, 2006.
5. J. Saleh: U.S. Patent, US 2004 0238086 Al, 2004.
6. DIN EN 50149; VDE 0115-602:2010-04: *European Standard* EN 50149, 2010.
7. J.C. Park, K.H. Han, S.K. Kim, Y.J. Yoon, D.K. Kim, and E.S. Joo: European Patent, No. EP 0772882. European Patent Office, Munich, Germany, 1997.
8. K. Maki, Y. Ito, H. Matsunaga, and H. Mori: *Scripta Mater*., 2013, vol. 68, pp. 777–80.
9. R. Schouwenaars, J.A. Torres, V.H. Jacobo, and A. Ortiz: *Mater. Sci. Forum*, 2007, vols. 539–543, pp. 317–22.
10. R. Schouwenaars, E.I. Ramírez, J. Romero, V.H. Jacobo, and A. Ortiz: *Eng. Fail. Anal*., 2012, vol. 25, pp. 175–81.
11. U.S. Environmental Protection Agency: EPA 430-R-08-008, 2008.
12. J.R. Davis: *ASM Specialty Handbook, Copper and Copper alloys*, ASM International, Metals Park, OH, 2001, pp. 43, 453–563.
13. X.J. Liu, C.P. Wang, I. Ohnuma, R. Kainuma, and K. Ishida: *Metall. Mater. Trans. A*, 2004, vol. 35A, pp. 1641–54.
14. F. Kohler, T. Campanella, S. Nakanishi, and M. Rappaz: *Acta Mater*., 2008, vol. 56, pp. 1519–28.
15. F. Kohler, L. Germond, J.D. Wagnière, and M. Rappaz: *Acta Mater*., 2009, vol. 57, pp. 56–68.
16. S. Fürtauer, D. Li, D. Cupid, and H. Flandorfer: *Intermetallics*, 2013, vol. 34, pp. 142–47.
17. D. Li, P. Franke, S. Fürtauer, D. Cupid, and H. Flandorfer: *Intermetallics*, 2013, vol. 34, pp. 148–58.
18. J.S. Park, C.W. Park, and K.J. Lee: *Mater. Charact*., 2009, vol. 60, pp. 1268–75.
19. A. Bravo, R. Schouwenaars, V.H. Jacobo, and A. Ortiz: *Mater. Sci. Forum*, 2010, vols. 654–656, pp. 1393–96.
20. L. Rokhlin and E. Lysova: *Selected Systems from Al-Si-Li to Ni-Si-Ti*, vol. 11 A4, Landolt-Börnstein Group IV Physical Chemistry, Springer, Berlin, 2006, pp. 238–47.
21. E.E. Vicente, S. Bermudez, A. Esteban, R. Tendler, B. Arcondo, and H. Sirkin: *J. Mater. Sci*., 1991, vol. 26, pp. 1327–32.
22. E.E. Vicente, S. Bermudez, R. Tendler, B. Arcondo, and H. Sirkin: *J. Mater. Sci. Lett*., 1996, vol. 15, pp. 1690–96.
23. J. Miettinen and G. Vassilev: *J. Min. Metall. Sect. B*, 2012, vol. 48(1)B, pp. 53–62.
24. M. Rappaz, F. Kohler, J. Valloton, A.B. Phillion, and M. Stampanoni: *Metall. Mater. Trans. A*, 2010, vol. 41A, pp. 563–67.
25. R.W. Cahn and P. Haasen, eds.: *Physical Metallurgy*, 4th ed., vol. 1, North Holland, Amsterdam, 1996, p. 312.
26. K. Osamura and Y. Murakami: *J. Less Common Met*., 1978, vol. 60, pp. 311–13.
27. G.R. Anstis, P. Chantikul, B.R. Lawn, and D.B. Marshall: *J. Am. Ceram. Soc*., 1981, vol. 64, pp. 533–38.
28. K. Niihara, R. Morena, and D.P.H. Hasselman: *J. Mater. Sci. Lett*., 1982, vol. 1, pp. 13–16.